PHYSICAL REVIEW B **79**, 104207 (2009)

Early stages of α-α' phase separation in Fe-Cr alloys: An atomistic study

G. Bonny,[1,2,*] D. Terentyev,[1] L. Malerba,[1] and D. Van Neck[2]
[1]*Nuclear Materials Science Institute, SCK-CEN, Boeretang 200, B-2400 Mol, Belgium*
[2]*Center for Molecular Modeling, Ghent University, Proeftuinstraat 86, B-9000 Gent, Belgium*

(Received 17 September 2008; revised manuscript received 5 December 2008; published 24 March 2009)

The thermal aging of Fe-Cr alloys was simulated using atomistic kinetic Monte Carlo techniques. The study was performed varying the Cr content in the range of 12–18 at. % Cr and at temperatures within the miscibility gap, where α-α' phase separation occurs. The evolution of the phase-separation process was characterized in terms of precipitate shape, composition, density, and mean size. The results offer a description of α-α' phase separation in its early stage, which is hardly accessible to experiments and of key importance in understanding the change in mechanical properties of Fe-Cr alloys under thermal aging. The critical size for a stable precipitate was estimated from the simulation data in the framework of Gibbs's homogeneous nucleation theory. The obtained results are compared, whenever possible, with available experimental data and the reliability, as well as the shortcomings, of the applied method is discussed accordingly. Despite strong oversimplifications, the used model shows good agreement with experimental data.

DOI: 10.1103/PhysRevB.79.104207 PACS number(s): 64.75.Nx, 64.70.K−, 81.30.−t, 64.60.Q−

I. INTRODUCTION

Fe-Cr alloys are the base for ferritic and ferritic/martensitic (F&FM) steels, which have a wide range of applications as structural materials in aggressive high-temperature environments, such as gas turbines in conventional power plants or key components in future nuclear reactors. Binary Fe-Cr alloys and F&FM steels undergo α-α' phase separation if the Cr content x_{Cr} exceeds ~9% in the region of temperatures potentially important for technological applications (>600 K).[1–10] The formation of finely dispersed nanometric-size Cr-rich precipitates in the bulk and at dislocations is long known to be the cause of hardening and embrittlement of F&FM steels with $x_{\mathrm{Cr}} > 14\%$ after thermal aging (475 °C embrittlement[1–5]), as well as, at even lower temperature and Cr content, under irradiation, which is found to accelerate the phase-separation process[7,9,10] or possibly induce it.[11–13] Therefore, a quantitative understanding of the kinetics of α-α' decomposition and its impact on mechanical property changes in Fe-Cr alloys must be pursued.

Experiments involving thermal aging are time consuming (years), especially at relatively low temperature and x_{Cr} close to the solubility limit. Tracing experimentally the kinetics of the unmixing from its very first stage is not trivial because: (i) the precipitates are coherent with the matrix, (ii) they are not pure and contain about 5–15 at. % Fe,[1–3,9,10,14–16] and (iii) the background concentration of the matrix material that experienced phase separation is at least 8 at. % Cr,[17–21] i.e., the depleted matrix is still a concentrated alloy. Due to the negligible strain field, transmission electron microscopy (TEM) experiences difficulties in detecting coherent precipitates of nanometric size.[9,10] More appropriate techniques, such as tomographic atom probe (TAP) and small-angle neutron scattering (SANS), also have drawbacks. TAP may not be fully reliable for the identification of the actual Cr concentration in the precipitates and requires corrections.[22] SANS has been extensively used to study α-α' unmixing in Fe-Cr (e.g., Refs. 6 and 8–10), but this technique provides no information about the morphology of precipitates in real space[23] and requires assumptions (e.g., about precipitate composition) to extract quantitative information from the obtained spectra.[6,8–10] For a rigorous and reliable study, different experimental techniques should therefore be combined, which is an expensive and time-consuming procedure. As a matter of fact, very few experimental works providing detailed information about α-α' precipitation in Fe-Cr alloys are available in the literature up to now, particularly for the range of compositions of technological application in power plants, i.e., <20 at. % Cr. Most work has been devoted to the study of spinodal decomposition in the model alloys with Cr content well above the F&FM steel composition (see Ref. 23 and references therein for a review).

Computer simulations seem therefore to be an attractive solution to complement the available experimental data, especially for the alloys with <20 at. % Cr and temperature below 800 K, where little or no experimental data are available. For a correct description of the diffusion process an atomistic description is necessary, from which the precipitate composition and morphology follows naturally.

Atomic-level computer simulations of Cr precipitation in Fe-Cr alloys have been proposed in Refs. 24 and 25. In the former, a rigid lattice cluster expansion (CE) and an exchange Monte Carlo (MC) approach were used to study the precipitate morphology qualitatively. In the latter, an interatomic potential and off-lattice Monte Carlo in transmutation ensemble were used to quantify the short-range-order (SRO) parameter as a function of Cr content and temperature. However, neither work provides information about the kinetics of the precipitation process. In particular, the different stages of nucleation, growth, and coarsening could not be distinguished.

In addition, the precipitates obtained in both works consist of pure Cr, which is contradictory to experimental observations.[1–3,9,10,14–16]

We apply here a classical rigid lattice atomistic kinetic Monte Carlo (AKMC) approach to simulate the thermal aging of Fe-Cr alloys. The point-defect migration barriers as a function of the local atomic environment (LAE) are evaluated on the fly using a density-functional theory (DFT)-based interatomic potential to describe the energetics of the system. The precipitates resulting from these simulations contain a few percents of Fe, in agreement with experimental measurements. To identify them from the Fe-Cr background, a method described in Ref. 26 is applied. Alloys in the composition and temperature ranges of 12–18 at. % Cr and 600–800 K were studied with the purpose of: (i) tracing the evolution of precipitate number density and mean size, as well as of the Cr concentration in the matrix, as a function of annealing time, varying temperature and Cr content; and (ii) characterizing the precipitates in terms of shape, composition, and critical size for nucleation. The results obtained are meant to be used later for the study of the precipitate hardening mechanisms in Fe-Cr alloys by means of molecular dynamics (MD). In addition, we performed simulations in the Fe-20Cr alloy in order to compare the results of our model with the few available experimental data, where information about the kinetics of the phase-separation process is provided. We find very reasonable agreement, despite the oversimplification of the model, as discussed in Sec. III C. The limitations inherent to the technique itself are also discussed in Sec. IV C.

II. COMPUTATIONAL DETAILS

A. Simulation of thermal aging

The thermal aging of the binary Fe-Cr alloys was modeled using a rigid lattice AKMC technique[27] implemented in the LAKIMOCA package.[28] Initially, the Cr atoms are randomly distributed in a body-centered-cubic (bcc) Fe matrix. The evolution of the system leading to the atomic redistribution is driven by single vacancy diffusion. The diffusion jump frequency of the vacancy, Γ, is evaluated as a thermally activated process, $\Gamma = \nu_0 \exp(-E_m/k_B T)$, where ν_0 is an attempt frequency chosen to be constant and equal to $6 \times 10^{12}\ \mathrm{s}^{-1}$, E_m is the LAE-dependent migration energy, k_B is the Boltzmann constant, and T is the absolute temperature. Note that *a priori* the attempt frequency ν_0 is also LAE dependent; however, this dependence can be neglected as compared to that of E_m since the latter appears in an exponent. In order to account for the LAE dependence of E_m, an algorithm adopting the Kang and Weinberg (KW) energy barrier decomposition (henceforth KW decomposition)[29] is used. This implies that $E_m = E_0 + \Delta E_{f-i}/2$, where ΔE is the total energy change after and before the jump and E_0 is the excess migration energy. ΔE is calculated on the fly using an interatomic potential as cohesive model (see Sec. II B). In order to enhance the computing speed, however, the energy of each atom is evaluated by including its interaction up to the third-nearest-neighbor (nn) shell only. As E_0, we choose the migration barrier of the atomic species exchanging position with the vacancy (Fe or Cr in our case), in the limit of infinitely dilute solution, as obtained from DFT calculations, namely, $E_0(\mathrm{Fe}) = 0.65$ eV and $E_0(\mathrm{Cr}) = 0.56$ eV.[30] In this simplified scheme E_0 is determined only by the migrating species, assuming that it has negligible dependence on the LAE, accounted for only in the ΔE term.[27,31] The assumption of LAE-independent E_0 has, however, some shortcomings that may be of importance and are briefly discussed in Sec. IV C. In addition, this model does not include vibrational entropy and magnetic disorder effects, which in principle are needed to reproduce correctly the experimental phase diagram.[32] As discussed in Sec. IV C, this is, however, not a major drawback for the temperature range considered here.

In a bcc lattice, there are eight possible first-nearest-neighbor sites where a single vacancy can jump to (exchanges with farther neighbors require much higher migration energy). In the model adopted here, each vacancy jump corresponds to a Monte Carlo step. The jump to be performed is chosen based on its probability, evaluated in terms of jump frequency. The time between two jumps is calculated according to a mean residence time algorithm, i.e., the inverse of the sum of the eight possible jump frequencies.[27]

The Cr content and simulation temperatures were chosen to be inside the miscibility gap where α-α' phase separation is expected and in the range of technological interest for nuclear applications: 12–18 at. % Cr and 600–800 K. Additional simulations were performed at 773 and 900 K for direct comparison with experiment (Sec. III C) and to provide additional data as explained in Secs. III A and IV A, respectively. The annealing processes were simulated up to $(1-2) \times 10^{10}$ MC steps (depending on temperature) when the coarsening regime was reached. This corresponded to a Monte Carlo simulation time t_{MC} of $\sim$130, 14, and 4 s for 600, 700, and 800 K, respectively. The correspondence between t_{MC} and the real annealing time in an experiment t_{real} is discussed in Sec. III C. The CPU time required by each simulation was on the order of 30 days. Each simulation was performed twice, with different seeds for the initial random distribution of Cr atoms and to start the sequence of Monte Carlo steps. Cubic boxes containing 128 000 atoms were used, which were checked to be adequate to avoid size effects on the energy evolution.

B. Choice of the cohesive model

The thermodynamic properties of Fe-Cr alloys are partially driven by a complex magnetic interaction,[33] which is challenging to model. Due to this magnetic interaction, a change in sign in the heat of mixing occurs, which is negative below a critical concentration and positive above it.[33–35] As a result, Cr atoms in the alloy may exhibit a tendency to order or to form clusters in the regions of negative and positive heat of mixing, respectively. Depending on the DFT approximations used, the critical concentration varies between 4 and 10 at. % Cr.[32,34,35] For our study, it is essential that the above-mentioned properties are well reproduced by the cohesive model implemented in the AKMC code.

In the literature there are to our knowledge only three cohesive models that, without explicitly including magnetism, nevertheless succeed in reproducing the Fe-Cr thermodynamic properties reasonably well. These are a concentration-dependent model (CDM) by Caro *et al.*,[36] a two-band model (2BM) by Olsson *et al.*,[37] and a cluster expansion model by Lavrentiev *et al.*[24] The former two formalisms are *ad hoc* extensions of the embedded atom method,[38] where an additional term dependent on local concentration was introduced. Since our objective is to use the results to

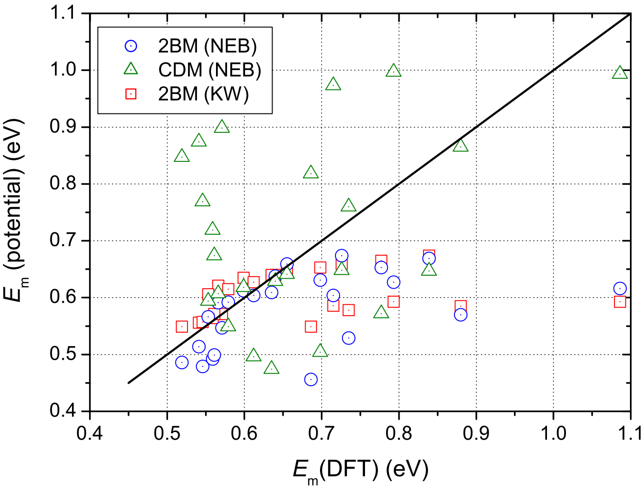

FIG. 1. (Color online) Comparison of migration barriers for different LAEs calculated by different methods.

perform MD simulations of the interaction of dislocations with Cr precipitates, the CE model is not suitable. In addition, such a model does not allow—should it be needed or possible in an AKMC framework—relaxation effects to be introduced.

Among the two potentials we opted for the 2BM since this model provides a phase diagram closest to the real one[32] when including vibrational entropy. Since vibrational entropy effects are not incorporated in the presently used rigid lattice model, the solubility is, as a consequence, underestimated at high temperature (≥900 K). In any case, at high temperature nonmagnetic models are expected to be less reliable, as discussed in Sec. IV C. Thus, the solubility limit underestimation provided by our model in that region is not a major shortcoming, as the model will not be used in that range. The incorrect description of the thermodynamic properties of the alloy at high temperature does not diminish the validity of the model in the appropriate range.

Another reason to choose the 2BM is that it provides a very good description of vacancy migration barriers (obtained for few different LAEs) when compared to existing DFT data,[39] as is presented in Fig. 1. The comparison with DFT of the migration barriers calculated from 2BM and CDM potentials, using the nudged elastic band (NEB) method,[40] shows that neither model provides a one to one agreement with the DFT values. However, the 2BM is clearly closer, especially for the low migration energy values, which correspond to the most frequent transitions. When comparing the NEB values with the KW decomposition results (superposed in Fig. 1), it can be seen that the difference is generally small, especially for low migration energy values. This partially justifies the adoption of the KW decomposition instead of more elaborate models, such as those sketched in Ref. 41.

Finally, the 2BM potential is the only cohesive model that predicts a composition of α' precipitates in a broad agreement with experimental observations,[26,32] suggesting that the precipitates contain a few percent of Fe,[1–3,9,10,14–16] rather than being pure Cr, as predicted by the other two models.[24,36] In summary, the choice of the cohesive model and of the migration energy expression was made based on transferability of the results to forthcoming works, consistency with experiment and DFT calculations, and as well as simplicity.

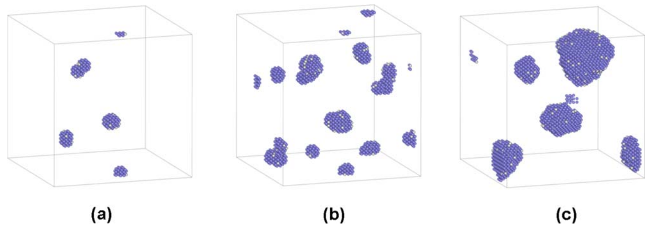

FIG. 2. (Color online) Snapshot of Fe-18Cr aged at 800 K at (a) the nucleation stage, (b) the peak density, and (c) coarsening stage. Cr atoms are plotted in dark (blue) and Fe atoms in bright (white).

C. Precipitate analysis

The atomic configurations from the AKMC simulations were postprocessed to identify and characterize the formed precipitates. A methodology presented in Ref. 26 that is capable of identifying nonpure coherent precipitates from a matrix containing also a high concentration of solute atoms has been applied. This technique is based on the idea of associating with each atom an on-site concentration obtained as the concentration within the *N*th-nearest-neighbor shell (here fifth nn). The precipitates are then identified as formed by all the lattice sites with a local concentration higher than or equal to a given threshold concentration (here 0.94, close to the Cr-rich phase boundary) augmented by all the surrounding lattice sites within *N*th-nearest-neighbor distance.

The volume V_p assigned to each precipitate was estimated as $V_p=N_p^{\text{at}}V_0$, where V_0 denotes the atomic volume and N_p^{at} is the number of atoms forming the precipitate. Assuming a spherical shape, the precipitate diameter d_p is estimated as $d_p=\sqrt[3]{6V_p/\pi}$ and the precipitate number density N_p (henceforth just density) is found as the ratio between the total number of precipitates and the total volume of the simulation box. Note that the applied procedure for the identification of the precipitates consistently excludes from the density count the very small Cr clusters, thereby spontaneously removing the problem of assigning a lower limit size to discriminate between precipitates and clusters. Based on the results of the model, an analysis aimed at unequivocally determining the critical radius for nucleation has subsequently been performed.

III. RESULTS

A. Size and density of precipitates

Applying the analysis described in Sec. II C, the precipitates were singled out from the Fe-Cr matrix during thermal annealing, as illustrated in Fig. 2, and their average diameter $\bar{d}_p$ and density N_p were determined as functions of t_{MC}. These quantities are presented in Figs. 3 and 4. In Fig. 5, x_{Cr} in the matrix and the precipitated atomic fraction f_p at the limiting temperatures studied here, i.e., 600 and 800 K for all simulated concentrations, are plotted as functions of t_{MC}. From these figures, the three regimes of the precipitation

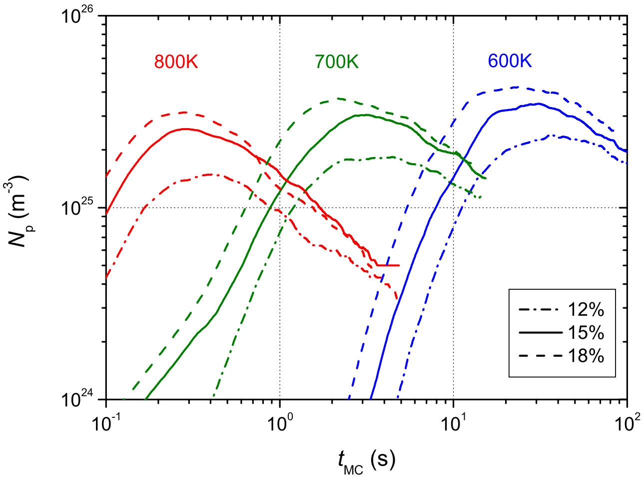

FIG. 3. (Color online) The precipitate density as a function of Monte Carlo simulation time.

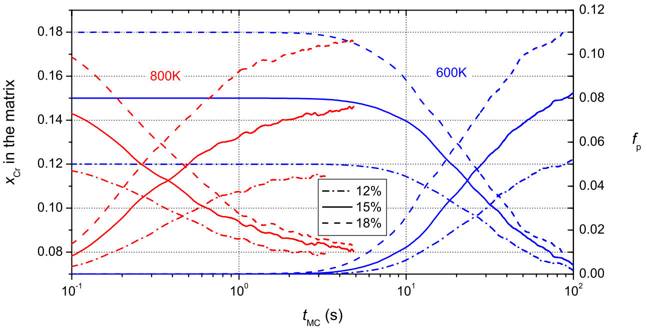

FIG. 5. (Color online) The Cr concentration in the matrix (decreasing curves) and the precipitate volume fraction (increasing curves) as functions of Monte Carlo simulation time.

process, namely, nucleation, growth, and coarsening can be identified. The initial steep increase in N_p and slow growth of $\bar{d}_p$ (Figs. 2 and 3) denote a dominant nucleation regime. The presence of the plateau around the peak density $N_p^{\max}$ and the simultaneous fast growth of $\bar{d}_p$ are to be attributed to the onset of the growth stage (the peak density versus temperature for all the simulated concentrations is shown in Fig. 6). Finally, the decrease in N_p and simultaneous increase in $\bar{d}_p$ with saturation of x_{Cr} in the matrix indicates the coarsening stage, at which larger precipitates grow at the cost of the dissolution (or coalescence) of smaller ones.

From the slopes of the N_p curves plotted in Fig. 3, it appears that the nucleation rate $\dot{N}_p$ increases with temperature, leading to a peak density that also increases with temperature. This dependence can be understood in terms of Gibbs's homogeneous nucleation theory;[42,43] according to which,

$$\dot{N}_p \propto \exp(-\Delta G_C/k_B T), \tag{1}$$

where ΔG_C is the critical free-energy barrier for nucleation, i.e., for the precipitate to become stable (see also below). From the slopes of the $\bar{d}_p$ curves it appears that the growth rate increases with temperature. This is consistent with the temperature dependence of the thermally activated self-diffusion mechanism controlling the precipitate growth, since the self-diffusion coefficient scales with temperature as $\exp(-E_a/k_B T)$, where E_a denotes the activation energy for self-diffusion. Finally, Fig. 6 shows that the peak density increases linearly with x_{Cr} and decreases with temperature. At peak time $\bar{d}_p$ stays constant at 1.4 ± 0.1 nm for all concentrations and temperatures studied. This means that at peak time only the density of the precipitates varies with concentration and temperature, not the size.

The clear identification of the three stages of the precipitation process and the agreement with theoretical considerations allow us to go further and use a combination of theory and simulation results to assess the critical free-energy barrier and cluster size for a precipitate to become stable. Assuming a homogeneous nucleation process, as is the case for

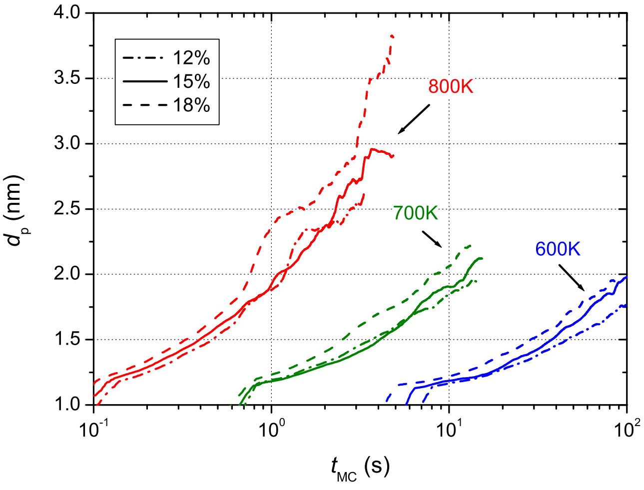

FIG. 4. (Color online) The average diameter of the precipitates as a function of Monte Carlo simulation time.

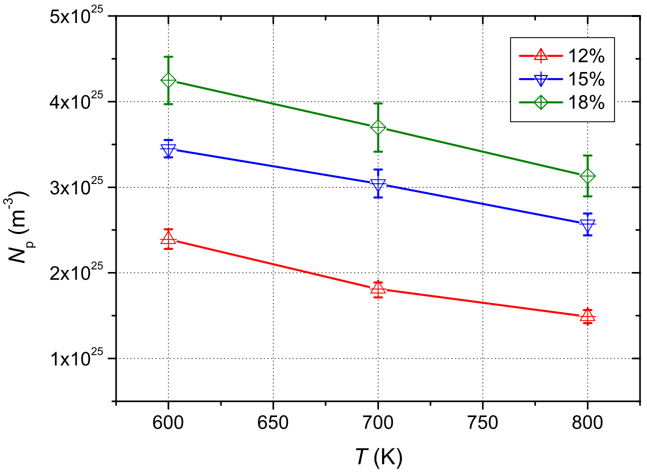

FIG. 6. (Color online) The precipitate density at peak time (i.e., highest density obtained in the simulation) as a function of temperature.

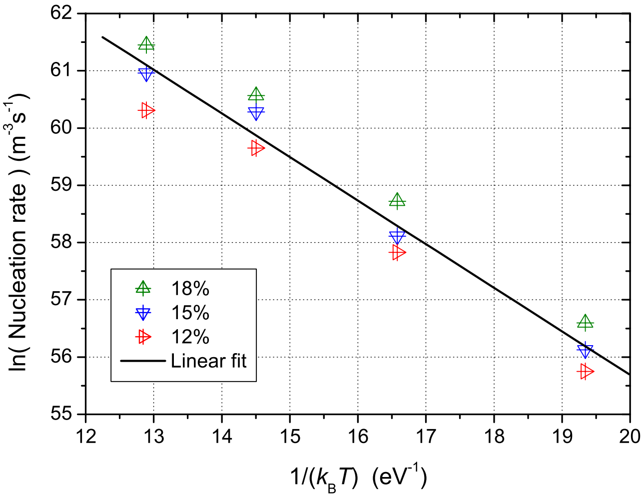

FIG. 7. (Color online) Arrhenius plot of the nucleation rate.

our simulations, because of the lack of imperfections (preferential sites for nucleation) in the AKMC crystallite, and considering that a spherical α'-precipitate forms in the metastable α matrix, the free-energy difference associated with this transformation is

$$\Delta G = \tfrac{4}{3}\pi R^3 \Delta g_c + 4\pi R^2 \sigma. \tag{2}$$

The first term is volume dependent and favors the formation of the precipitate because of the creation of the stable α' phase. The second one is a surface-dependent term counteracting the precipitate growth due to the creation of the α'-α interface. The free-energy difference per unit volume between the α' and α phases is denoted as Δg_c (a negative factor), σ denotes the α-α' interface energy, and R is the radius of the nucleus. It is clear from Eq. (2) that initially the free-energy difference increases due to the formation of an additional interface, but starting from a certain critical size it decreases due to the formed α' phase. The critical radius R_C at which a stable nucleus is formed is thus

$$R_C = \sqrt{\frac{3\Delta G_C}{4\pi\sigma}}, \tag{3}$$

where ΔG_C is the total free-energy change at the critical size from Eq. (2). A precipitate embryo with a radius larger than R_C (henceforth nucleus) will grow further because its growth leads to a further decrease in the free energy. At the steady state Eq. (1) holds. In Fig. 7, $\ln \dot{N}_p$, as obtained from the evolution of the precipitate density (see Fig. 3), is plotted versus the reciprocal of the k_BT product. The required critical free-energy difference $\Delta G_C = 16\pi\sigma^3/3\Delta g_c^2$ is independent of temperature, so it can be estimated from the slope of the straight line fitted to the data points in Fig. 7. A value of 0.76 eV is found for ΔG_C using a linear fit. The Fe-Cr interface energy was separately estimated to be about 5–10 meV/Å^2 (depending on the surface orientation), so R_C estimated from Eq. (3) is found to be about 0.6–0.4 nm. Note that in Fig. 7 we included data points obtained at 900 K too. At this T, our model still predicts precipitation, contrary to what should be expected from the experimental phase diagram, because of the absence of vibrational and magnetic effects in the model, as already mentioned and further discussed later on. The model is thus not valid there when compared to experiments. However, an additional point improves statistics to estimate the critical radius and free-energy barrier.

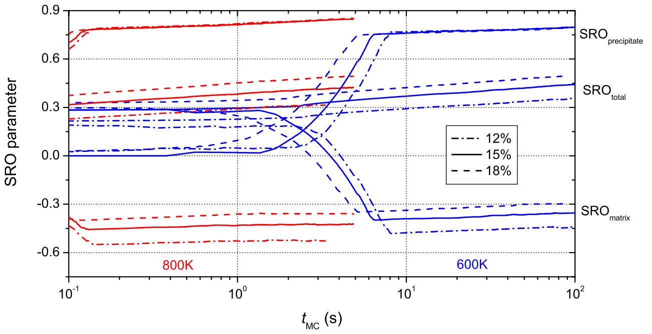

FIG. 8. (Color online) Partial and total SRO parameters as functions of Monte Carlo simulation time.

B. Atomic distribution in precipitates and matrix

The visualization of the precipitates extracted from the matrix, as illustrated in Fig. 2, revealed that the stable precipitates formed have indeed, as assumed above, roughly spherical shapes. After the nucleation stage, however, the boundaries of the precipitates are formed mainly by {110} facets for all x_{Cr} and T studied here, in agreement with the results obtained by Lavrentiev *et al.*[24]

To quantify the level of ordering in both α and α' phases, the Warren-Cowley SRO parameter[44] was calculated separately for the atoms located in the depleted matrix (henceforth α-SRO), in the precipitates (henceforth α'-SRO), and in the whole simulation crystal (henceforth total SRO parameter). The SRO parameter for the υth nn shell is defined as

$$\mathrm{SRO}^{(\nu)} = 1 - \frac{p_{\mathrm{FeCr}}^{(\nu)}}{x_{\mathrm{Fe}} x_{\mathrm{Cr}}}, \tag{4}$$

where x_{Fe} and x_{Cr} denote the global Fe and Cr concentrations, respectively. $p_{\mathrm{FeCr}}^{(\nu)}$ represents the mixed υth-nearest-neighbor pair probability. The SRO parameter measures the deviation at short range from the random state and vanishes for the purely random state. A positive SRO indicates a number of atomic pairs of the same type higher than in the random alloy, i.e., local clustering of alike atoms; a negative SRO parameter denotes, on the contrary, a number of pairs of unlike atoms higher than in the random state, expressing local ordering.

In Fig. 8 the two partial SROs and the total SRO parameters are plotted. The total SRO parameter remains positive during the whole precipitation process, due to the progressive clustering of Cr atoms. The α'-SRO parameter is also positive, while the α-SRO parameter is negative during the whole precipitation process, consistently with the results obtained in Ref. 25. The absolute values of the partial SRO parameters are actually meaningless due to matrix-precipitate interface effects, as explained in Ref. 25, but they are indicative of trends and they are the only ones comparable with

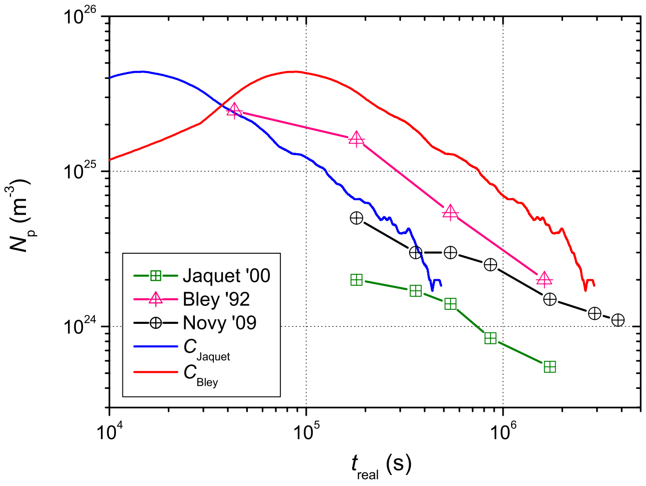

FIG. 9. (Color online) Comparison of experimental and simulated precipitate densities.

existing experimental measurements. The important observation from this figure is that all three SRO parameters quickly reach an almost constant asymptotic level. This means that the mixed pair probabilities in the matrix and in the precipitates, after a very short transient from the random state, do not change during the whole precipitation process from nucleation to coarsening. In other words, local equilibrium is always reached extremely fast.

C. Comparison with experiment

A direct comparison of AKMC simulations with thermal aging experiments is difficult due to the lack of a safe criterion to establish the correspondence between t_{real} and t_{MC}, as discussed, e.g., in Ref. 45. The solution proposed in that work is to use experimental data to establish the synchronization. However, in the present case the difficulty stems from the lack of experimental data. The closest experimental case to our simulations concerns relatively pure Fe-20Cr alloys aged at 773 K reported in Refs. 6, 8, and 21, where SANS and TAP techniques were used separately, on different specimens, to trace the precipitation evolution. The shortest studied aging time was 12, 20, and 50 h, respectively and from then on only the coarsening stage was observed. Additional AKMC simulations for Fe-20Cr aged at 773 K were therefore performed in order to be able to compare the results of our model with experimental data. The synchronization was established ($t_{\text{real}}=Ct_{\text{MC}}$) by determining the C value corresponding to the first time that the simulated diameter equals the experimental one. In the absence of full consistency between the experimental data, we determined two coefficients $C_{\text{Bley}}=4.15\times10^5$ and $C_{\text{Jaquet}}=6.92\times10^4$ using data from Refs. 6 and 8, respectively. The results for $\bar{d}_p$ and N_p after synchronization are presented and compared with the experimental data[6,8,21] in Figs. 9 and 10, respectively. It is clear that for both estimates of C reasonable agreement with experiment is reached. Note that the discrepancy between the three experiments, probably due to the ambiguity in the interpretation of the SANS data, is of the same order as the discrepancy between simulation results and any experimental data set.

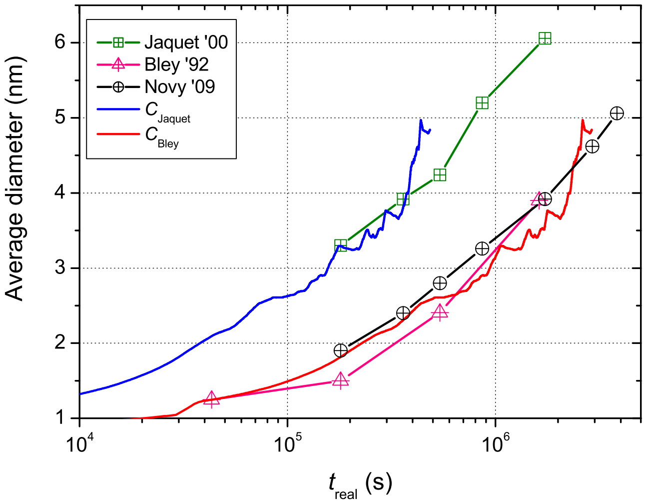

FIG. 10. (Color online) Comparison of experimental and simulated mean precipitate diameters.

As a cross check, we estimated the formation energy of a vacancy in the Fe-20Cr alloy according to the obtained conversion factors. The Monte Carlo simulation time can be related with real time using the following expression:[45]

$$t_{\text{real}}=\left(\frac{C_V^{\text{MC}}}{C_V^{\text{real}}}\right)t_{\text{MC}}, \tag{5}$$

where C_V^{real} and C_V^{MC} are the equilibrium thermal vacancy concentration and the vacancy concentration in the simulated crystal ($C_V^{\text{MC}}=1/128\,000$), respectively. The thermal equilibrium vacancy concentration is given as $C_V^{\text{real}}=K\exp(-E_f^V/k_BT)$, where E_f^V is the formation energy for a vacancy in the Fe-Cr alloy and K is a constant factor approximately equal to 3 due to the configurational entropy.[46] The identification of $C_V^{\text{MC}}/C_V^{\text{real}}$ with the above-obtained conversion factors yields the values of 1.76 and 1.64 eV for E_f^V, respectively. We now compare these values with the estimates from the self-diffusion experiments performed by Wolfe and Paxton.[47] We therefore extract the vacancy formation energy from the reported activation energies E_a, so that $E_f^V=E_a-E_0$. Using the values for E_0 given in Sec. II A, the formation energy for a vacancy is estimated to be around 1.68 eV for Fe-20Cr, which is in the range of the values estimated by synchronizing our simulation results to the experimental data. The fairly good agreement for $\bar{d}_p$ and N_p with the thermal aging experiments[6,8] and for the estimated vacancy formation energy with the results obtained in independent experimental self-diffusion measurements[47] makes us believe that our simulations provide an adequate description of Fe-Cr thermal aging up to the onset of the coarsening stage, within the studied x_{Cr} and for T up to 800 K. Above 800 K the Cr solubility predicted by the rigid lattice model underestimates the experimentally determined limit. (The data obtained at 900 K are only to be considered as a complement for the consistency check with the phase diagram, as explained in Sec. IV, and to provide extra data for

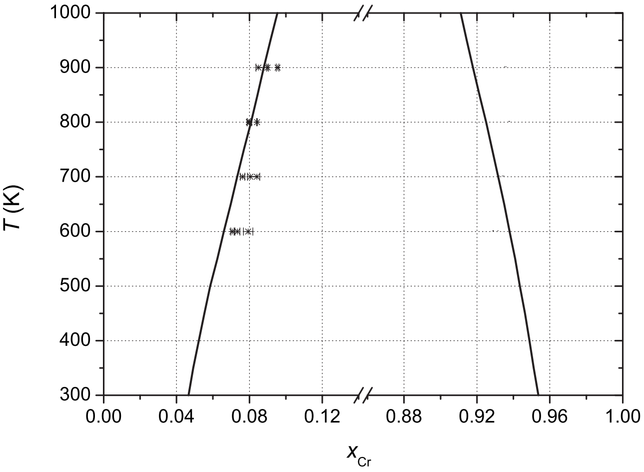

FIG. 11. The phase diagram estimated in regular solution approximation for the interatomic potential used in this work.

the estimation of the critical size for a stable precipitate, as already mentioned).

IV. DISCUSSION

A. Consistency with the phase diagram

In Fig. 11 the phase diagram obtained using regular solution approximation and the interatomic potential is plotted. We thus can verify whether the obtained results, regardless the approximations inherent to the applied AKMC method, converge to the thermodynamic limit predicted by the interatomic potential or not. It is important to verify that the thermodynamic limit is not changed significantly when applying the potential in AKMC method. The consistency of the phase diagram predicted by the potential with the experimental one is discussed in Ref. 32.

Focusing on the Cr-rich phase boundary in Fig. 11, which determines the α' composition in the thermodynamic limit, the precipitate composition appears to be about 92–94 at. % Cr in the temperature range of 600–800 K. This is in good agreement with the composition of α' precipitates estimated to be about 93–94 at. % Cr, as determined by the threshold (see Sec. II C). From Fig. 5, f_p obtained from the simulations can be compared with f_p predicted from the phase diagram using the lever rule. The comparison shows an agreement within 3 at. % for all temperatures and alloys studied. The phase boundary points determined from the AKMC simulations as described above are superposed in Fig. 11. We conclude that the results obtained by the rigid lattice AKMC are indeed consistent with the phase diagram calculated independently, with the same interatomic potential, in regular solution approximation (i.e., without including any vibrational entropy contribution).

B. Characterization of precipitates

In the range of x_{Cr} and T studied here, we found that the precipitation process occurs via nucleation, growth, and coarsening stages, clearly dominating at different moments during the simulation. The critical precipitate radius and free-energy barrier for the stable nucleus were estimated to be 0.4–0.6 nm and 0.76 eV, respectively, which suggests that only stable nuclei well above the critical size are resolvable by experimental techniques such as TEM. Caution should be taken, however, about the applicability of the homogeneous nucleation theory. Since magnetic and vibration effects may alter the interface-energy value, the estimated critical radius may change as well. However, within the fairly wide range of interface-energy values estimated for different surface orientations (see Sec. III A), we believe that the effect on the reported critical radius would be largely irrelevant.

It is important to mention that N_p at peak time is at least 1 order of magnitude larger than at the coarsening stage. This suggests that a comparison between simulation results and experiments may reveal apparent discrepancies if the simulation is short and the experiments well into the coarsening stage, especially in the absence of a clear criterion to perform the time renormalization.[45] This point is further discussed in Sec. IV C.

Finally, the peak density decreases linearly with temperature and increases with concentration, as shown in Fig. 6, while $\bar{d}_p$ remains the same within the error bar at 1.4 ± 0.1 nm. As a consequence, the hardening related to the presence of precipitates at the end of the nucleation stage is expected to be determined mainly by the density.

C. Limitations of the simulations

The AKMC model applied here to trace the stages of α-α' separation is oversimplified from many points of view. In particular, no contribution to the free energy of the system from relaxation and magnetic effects is included, as we use a rigid lattice approximation and a classical interatomic potential as cohesive model. The latter was fitted to the ferromagnetic enthalpy of the alloy obtained from DFT, i.e., at 0 K and thus cannot reproduce the magnetic transition. To be on the safe side, the model should therefore only be used at temperatures well below the Curie temperature ($\approx$1000 K),[18] where magnetic disorder has a minor effect on the Cr solubility. For example, as remarked already, the model predicts precipitation at 900 K, whereas this is not observed in experiments.

Furthermore, the use in the KW decomposition[29] of a LAE-independent excess migration energy to estimate the LAE-dependent migration barriers is known *a priori* to be an oversimplification, as shown for example by Djurabekova *et al.*[41] However, the comparison of the barriers estimated using the NEB method and the KW decomposition, presented in Fig. 1, reveals that the deviations are not significant, especially for low values of the migration barriers, which are of primary importance. Moreover, low migration energy barriers from the KW decomposition also show reasonable agreement with the available DFT values.[39]

Another restriction of the AKMC used here is the constant attempt frequency prefactor ν_0. Due to the temperature dependence of vibrational and magnetic entropy, ν_0 is also temperature dependent, an effect which is not accounted for here. Stated this, however, the LAE dependence of the migration barriers is a more important effect.[41]

The main advantage of the model presently adopted is that it combines simplicity and effectiveness at describing the *kinetics* of α-α' separation in concentrated Fe-Cr alloys, while accounting for the latest information from DFT calculations about the thermodynamic properties of this alloy. Nonetheless, there are limitations inherent to the AKMC technique itself, independently of the adopted cohesive model and algorithm for the migration energy estimation. From the results presented above, it appears that N_p (estimated to be between 2×10^{24} and $3\times10^{25}\ \mathrm{m}^{-3}$) is larger compared to typical experimental data ($10^{22}-10^{23}\ \mathrm{m}^{-3}$) from TEM observations.[9,10] On the other hand, $\bar{d}$ estimated near the end of the simulation remains rather small (3–4 nm), just above the limit of the TEM resolution. As suggested by Figs. 9 and 10, one needs to prolong the simulations by a few orders of magnitude in time to obtain densities and sizes in the experimental range, which is therefore outside our current computational capabilities. An additional problem is represented by the absence of a safe criterion to renormalize the simulation time. It should be noted that the use of a self-consistent approach based on the idea of parametrizing Eq. (5) using estimates from the model itself, such as the one suggested in Ref. 48, is only applicable in the case of dilute alloys. For example, in concentrated alloys there is no one precise value for the formation energy of a vacancy, but an average value that can be only obtained *a posteriori* after proper averaging over a large number of local configurations, or deduced indirectly, as done here in Sec. III C. Thus, an approach based on the synchronization with experimental data, as suggested in Ref. 45, is the only option. However, such a synchronization becomes impossible if there is no single simulation point overlapping with the experimental points.

Furthermore, the minimum density and maximum obtainable size are limited by the simulation box size. For the chosen simulation crystal, the possible lowest density (one precipitate per box) is $6.7\times10^{23}\ \mathrm{m}^{-3}$. Using the lever rule at 600–800 K for Fe-12Cr, the maximum possible f_p is estimated at 0.062–0.046 and 0.131–0.117 for Fe-18Cr at 600 and 800 K, respectively. Assuming one spherical precipitate per box and using the just-estimated precipitated fractions, the maximum precipitate diameter in Fe-12Cr would be 5.6–5.1 nm at 600–800 K and 7.2–6.9 nm in Fe-18Cr at 600–800 K, respectively. This suggests that, at the coarsening stage, size effects may come into play, biasing the results toward lower sizes and higher densities of the precipitates.

It is important to note that the CPU time shows a quadratic increase with box volume.[49] We therefore believe that AKMC simulations, as performed in this study, are in fact not an adequate tool to study the coarsening process in the Fe-Cr system. Advanced methods, possibly exploiting parallelization techniques and other specific algorithms to reduce the computational load, are certainly needed to allow AKMC simulations to treat correctly a coarsening process in concentrated alloys.

We believe, however, that the nucleation and growth stages can be adequately reproduced, even using an oversimplified model such as ours, as long as the thermodynamics and defect mobilities in the alloy are acceptably reproduced. At these stages, the mean precipitate size is small (a few nanometer), while the density is high, in agreement with experiments, as shown in Sec. III C. They are therefore accessible to AKMC techniques. Another indirect prove of this is the fact that the critical size found here is below the resolution of experimental techniques (<1.2 nm), so the precipitates observed experimentally are stable ones. In turn, this means that the simulation results provide a correct upper bound for the stable precipitate size.

V. CONCLUSIONS

A simple rigid lattice AKMC approach has been applied to study the precipitation process in Fe-Cr alloys varying Cr content and temperature. The precipitation process has been characterized in terms of precipitate shape, size, density, and internal structure. The rearrangement of Cr solutes in the depleting matrix was followed by estimating partial and total SRO parameters during the precipitation process. The obtained results have shown that the precipitation process in the studied alloys occurs in three stages, namely, nucleation, growth, and coarsening and that the applied model is adequate to reproduce the first two.

The critical size for stable precipitates was determined to be less than 1.2 nm, which is at the limit of the resolution of many experimental techniques. The maximum density was found to vary with temperature and Cr content, but the average precipitate size (at the moment when the maximum density is reached) remains the same ($\bar{d}_p=1.4$ nm) within the error of the calculations.

The comparison of the precipitate size and density with experimental data showed reasonable agreement, despite of the oversimplification of the model, which does not allow for vibrational and magnetic effects. We therefore believe that the presented results can serve to describe the evolution of the precipitation process in its early stages at temperatures below Curie temperature, on which the experimental observation techniques hitherto applied have provided hardly any data.

ACKNOWLEDGMENTS

The research leading to these results has received partial funding from the European Atomic Energy Community 7th Framework Programme (FP7/2007-2011) under Grant Agreement No. 212175 (GetMat project). These results also contribute to the European Fusion Programme coordinated by the EFDA Fusion Materials Topical Group. The authors thank D. Nguyen-Manh and M. Yu. Lavrentiev for providing details on their DFT calculations and useful discussions during the preparation of this work.

[*] Corresponding author; gbonny@sckcen.be

[1] R. M. Fisher, E. J. Dulis, and K. G. Carroll, Trans. AIME **197**, 690 (1953).
[2] R. O. Williams and H. W. Paxton, J. Iron Steel Inst., London **185**, 358 (1957).
[3] R. Lagneborg, Trans. ASME, J. Dyn. Syst. Meas. **60**, 67 (1967).
[4] P. J. Grobner, Metall. Trans. **4**, 251 (1973).
[5] P. Jacobsson, Y. Bergström, and B. Aronsson, Metall. Trans. A **6A**, 1577 (1977).
[6] F. Bley, Acta Metall. Mater. **40**, 1505 (1992).
[7] P. Dubuisson, D. Gilbon, and J. L. Séran, J. Nucl. Mater. **205**, 178 (1993).
[8] V. Jaquet, Ph.D. thesis, Ecole Polytechnique, Palaiseau, France, 2000.
[9] M. H. Mathon, Y. De Carlan, G. Geoffroy, X. Averty, C. H. de Novion, and A. Alamo, in *Effects of Radiation on Materials: 20th International Symposium*, ASTM STP 1405, edited by S. T. Rosinski, M. L. Grossbeck, T. R. Allen, and A. S. Kumar (American Society for Testing and Materials, West Conshohocken, PA, 2001), p. 674.
[10] M. H. Mathon, Y. de Carlan, G. Geoffroy, X. Averty, A. Alamo, and C. H. de Novion, J. Nucl. Mater. **312**, 236 (2003).
[11] E. A. Little and D. A. Stow, J. Nucl. Mater. **87**, 25 (1979).
[12] E. Wakai, A. Ishinuma, Y. Kato, H. Yano, S. Takaki, and K. Abiko, J. Phys. IV **5**(C7), 277 (1995).
[13] E. Wakai, A. Hishinuma, K. Usami, Y. Kato, S. Takaki, and K. Abiko, Mater. Trans., JIM **41**, 1180 (2000).
[14] S. S. Brenner, M. K. Miller, and W. A. Soffa, Scr. Metall. **16**, 831 (1982).
[15] H. Kuwano, Trans. Jpn. Inst. Met. **26**, 473 (1985).
[16] S. M. Dubiel and G. Inden, Z. Metallkde. **78**, 544 (1987).
[17] O. Kubaschewski, *Iron Binary Phase Diagrams* (Springer, Berlin, 1982).
[18] J.-O. Andersson and B. Sundman, CALPHAD: Comput. Coupling Phase Diagrams Thermochem. **11**, 83 (1987).
[19] T. B. Massalsky, H. Okamoto, P. R. Subramanian, and L. Kacprzac, *Binary Alloy Phase Diagrams* (ASM International, Materials Park, OH, 1990), p. 1273.
[20] G. Bonny, D. Terentyev, and L. Malerba, Scr. Mater. **59**, 1193 (2008).
[21] S. Novy, P. Pareige, and C. Pareige, J. Nucl. Mater. **384**, 96 (2009).
[22] J. M. Hyde, M. K. Miller, A. Cerezo, and G. D. W. Smith, Appl. Surf. Sci. **87-88**, 311 (1995).
[23] F. Danoix and P. Auger, Mater. Charact. **44**, 177 (2000).
[24] M. Y. Lavrentiev, R. Drautz, D. Nguyen-Manh, T. P. C. Klaver, and S. L. Dudarev, Phys. Rev. B **75**, 014208 (2007).
[25] P. Erhart, A. Caro, M. Serrano de Caro, and B. Sadigh, Phys. Rev. B **77**, 134206 (2008).
[26] G. Bonny, D. Terentyev, and L. Malerba, Comput. Mater. Sci. **42**, 107 (2008).
[27] W. M. Young and E. W. Elcock, Proc. Phys. Soc. London **89**, 735 (1966).
[28] C. Domain, C. S. Becquart, and J. C. Van Duysen, Mater. Res. Soc. Symp. Proc. **650**, R3.25.1 (2001).
[29] H. C. Kang and W. H. Weinberg, J. Chem. Phys. **90**, 2824 (1989).
[30] P. Olsson, C. Domain, and J. Wallenius, Phys. Rev. B **75**, 014110 (2007).
[31] E. W. Elcock, Proc. Phys. Soc. London **73**, 250 (1959).
[32] G. Bonny, R. C. Pasianot, L. Malerba, A. Caro, P. Olsson, and M. Yu. Lavrentiev, J. Nucl. Mater. **385**, 268 (2009).
[33] T. P. C. Klaver, R. Drautz, and M. W. Finnis, Phys. Rev. B **74**, 094435 (2006).
[34] P. Olsson, I. A. Abrikosov, and J. Wallenius, J. Nucl. Mater. **321**, 84 (2003).
[35] P. Olsson, I. A. Abrikosov, and J. Wallenius, Phys. Rev. B **73**, 104416 (2006).
[36] A. Caro, D. A. Crowson, and M. Caro, Phys. Rev. Lett. **95**, 075702 (2005).
[37] P. Olsson, J. Wallenius, C. Domain, K. Nordlund, and L. Malerba, Phys. Rev. B **72**, 214119 (2005).
[38] M. S. Daw and M. I. Baskes, Phys. Rev. B **29**, 6443 (1984).
[39] D. Nguyen-Manh, M. Yu. Lavrentiev, and S. L. Dudarev, C. R. Phys. **9**, 379 (2008).
[40] H. Jonsson, G. Mills, and K. W. Jacobsen, in *Nudged Elastic Band Method for Finding Minimum Energy Paths of Transitions*, Classical and Quantum Dynamics in Condensed Phase Simulations, edited by B. J. Berne, G. Ciccotti, and D. F. Coker (World Scientific, Singapore, 1998).
[41] F. G. Djurabekova, R. Domingos, G. Cerchiara, N. Castin, E. Vincent, and L. Malerba, Nucl. Instrum. Methods Phys. Res. B **255**, 8 (2007).
[42] J. W. Gibbs, Trans. Conn. Acad. Arts Sci. **3**, 102 (1878).
[43] J. W. Martin, *Micromechanisms in Particle-Hardened Alloys* (Cambridge University Press, Cambridge, England, 1980).
[44] J. M. Cowley, Phys. Rev. **77**, 669 (1950).
[45] E. Vincent, C. S. Becquart, C. Pareige, P. Pareige, and C. Domain, J. Nucl. Mater. **373**, 387 (2008).
[46] D. A. Porter and K. E. Easterling, *Phase Transformations in Metals and Alloys*, 2nd ed. (CRC, Cheltenham, UK, 1992).
[47] R. A. Wolfe and H. W. Paxton, Trans. Metall. Soc. AIME **230**, 1426 (1964).
[48] F. Soisson and C.-C. Fu, Phys. Rev. B **76**, 214102 (2007).
[49] A. Chatterjee and D. G. Vlachos, J. Comput.-Aided Mater. Des. **14**, 253 (2007).